Lymphology 47 (2014) 164-176

IDENTIFICATION AND DESCRIPTION OF THE AXILLARY WEB SYNDROME (AWS) BY CLINICAL SIGNS, MRI AND US IMAGING

O. Leduc, E. Fumière, S. Banse, C. Vandervorst, A. Clément, T. Parijs, F. Wilputte, F. Maquerlot, M. Ezquer Echandia, A. Tinlot, A. Leduc

Lympho-Phlebology Unit (OL,SB,CV,AT,AL), Department of Occupational and Environmental Physiology, Haute Ecole P. H. Spaak, Brussels; Department of Radiology (EF), Vesale Hospital Charleroi, Montigny le Tilleul, Belgium; Isala Breast Unit and Prevention Center (AC). Saint Pierre University Hospital (ULB-VUB), Brussels; Department of Vascular Surgery (TP), Iris Sud Hospital Ixelles, Brussels; Department of Vascular Pathology (FW), Erasme Hospital, Academic Medical Center of the ULB, Université Libre de Bruxelles, Brussels; Private Center of Physiotherapy (FM,MEE), Treatment of Edema, Brussels, Belgium

ABSTRACT

The Axillary Web Syndrome (AWS) follows surgery for breast neoplasia and consists of one, or more frequently two or three, cords of subcutaneous tissue. Cords originate from the axilla, spread to the antero-medial surface of the arm down to the elbow and then move into the antero-medial aspect of the forearm and sometimes into the root of the thumb. The purpose of this study was to compare two techniques, ultrasound (US) and Magnetic Resonance Imaging (MRI) for their sensitivity and accuracy in identifying AWS cords and to provide insights to the origin of this pathology. US examinations were performed on fifteen patients using a high frequency probe (17MHz). We first palpated and marked the cord with location aided by maximum abduction. To identify the cord with MRI (1.5 Tesla), a catheter filled with a gel detectable under MRI was placed on the skin at the site of the cord. We found that in some US cases, the dynamic abduction maneuver was essential to facilitate detection of the cord. This dynamic method on ultrasound confirmed the precise location of the cord even if it was located deeper in the hypodermis fascia junction. US and MRI images revealed features of the cords and surrounding tissues. Imaging the cords was difficult with either of the imaging modalities. However, US seemed to be more efficient than MRI and allowed dynamic evaluation. Overall analysis of our study results supports a lymphatic origin of the AWS cord.

Keywords: axillary web syndrome, lymphatic, cords, ultrasound, Magnetic Resonance Imaging, breast cancer, axillary node dissection

Axillary Web Syndrome (AWS), also called "syndrome of the axillary cords" was first described in 2001 by Moskovitz et al (1). This description was confirmed by Leidenius et al. in 2003 (2) and by Reedijk et al in 2006 (3). This syndrome follows surgery for breast neoplasia and consists in the appearance of one (or more frequently two or three) cords of subcutaneous tissue. Cords originate from the axilla, spread to the antero-medial surface of the arm down to the elbow and then move into the antero-medial aspect of the forearm and sometimes into the root of the thumb. AWS is also characterized by a reduced mobility of the upper limb in abduction and flexion of the shoulder and by pain when the cords are in tension (1-4). AWS appears within one to eight weeks after surgery, usually between the second and third post-operative week and resolves spontaneously within three months (1-5). Nevertheless, some authors assert that the AWS can be resolved in less than three months if taken care of by physiotherapy (5-7). AWS mostly develops as a result of an axillary dissection and more rarely after application of the sentinel node technique (1,2,7). Worthy of note is that no cases of AWS have been listed after limited breast surgery in the absence of axillary lymph node dissection (1,2,3,5).

In 2009, we published evidence (5) to confirm the hypothesis put forward by Moskovitz et al in 2001 (1) that "a reduction in tissue damage by more limited surgery may reduce the incidence and severity of the AWS." They reported that less tissue damage through less invasive surgery of the axilla and of the lymphatic structures could reduce the severity of movement limitations as well as the extent of the cord. There are several hypotheses regarding the etiology of the syndrome: a disturbance or anomaly of the lympho-venous or lymphatic structures (1,3-5,8), of fascia (9), of nerves (1) of other tissues (10,11). Some of these proposals have been confirmed, but none has been formally demonstrated. To date, medical imaging of AWS cords has to our knowledge not been described in the literature.

The aim of our study was to identify the nature of AWS by comparing clinical findings with US and MRI imaging.

MATERIALS AND METHODS

The study was conducted in collaboration with the Vesale University Hospital of Charleroi in agreement with the ethics committee of the hospital. After being informed of the procedures of the study, all patients gave their written informed consent. In total, fifteen patients were included in the study, fourteen women (W) and one man (M) aged 37 to 67 years (mean age 52 years). They completed a questionnaire with general information as well as information on the cords and possible contraindications to MRI.

The study inclusion criteria consist of:

- Presence of one or more cord(s) appearing postoperatively
- BMI between 18 and 25
- No contraindication against MRI.

Exclusion criteria:

- BMI over 25 with impalpable cord(s)
- Presence of contraindications to MRI
- Claustrophobia

Six patients underwent a lumpectomy, four (W) with axillary dissection and two (W) with the sentinel node technique. Mastectomy with axillary dissection was performed in nine other patients (8W/1M).

Ultrasound

Examinations were performed using a Philips iU22 ultrasound with a high frequency probe (17MHz). We first palpated and marked the cord. Shoulder abduction was sometimes necessary to view the cord(s) that were, in some cases, difficult to detect without this maneuver. The examiner then applied a liquid gel as well as a gel plate pad SONAR AID on the area to be examined in order to enhance the contrast and make the images more uniform. A probe was placed on the skin above the cord to facilitate visualization.

Magnetic Resonance Imaging

To identify the cord, a catheter filled with a gel detectable under MRI was placed on the skin at the site of the cord. The equipment used was a 1.5 Tesla AVANTO (SIEMENS) MRI. The patient was placed in the supine position: head first, arms along the body. The examiner performed sequences in order to capture the cord.

TABLE 1
Summary of Features Identified with US Imaging of Cords and Surrounding Tissues in 15 Patients

	*P1	P2	P3	P4	P5	P6	P7	P8	P9	P10	P11	P12	P13	P14	P15
Appearance of vessels with anechoic light		x			x	x			x	x	x	x			
No light								x							
Hyperechogenic cord		x		x				x			x	x		x	x
Fibrous scar							x								
Several cords		x								x					
Hyperechogenic edematous infiltration		x				x				x			x		
Intraluminal thrombus	x	x			x	x			x	x	x			x	
Dermo hypodermic junction	x		x	x	x	x		x						x	
Juxta-aponeurotic									x	x					
Hypodermis		x					x				x	x	x		x
Resting arch	x					x	x		x						
Arch during the tensioning	x	x		x	x	x		x				x		x	
No flow on Doppler		x			x	x			x	x					
Unrealized Doppler	x		x	x			x	x			x	x	x	x	x

*P = Patient

For each patient, the sequences below were carried out:

- Coronal Spin Echo (SE) T1 (Slice Thickness (ST) :5 mm, Echo Time (TE) :10 msec, Repetition Time (TR) : 585 msec, Field of view (FOV): 400 * 400 mm, Matrix: 512 * 512)
- Coronal Short Time Inversion Recovery (STIR) (ST: 5 mm, TE: 36 msec, TR : 4300 msec, FOV: 400 * 400 mm, Matrix: 256 * 256)
- Axial SE T1 (ST : 5 mm, TE :10 msec, TR : 470 msec, FOV: 300 * 300 mm, Matrix: 358 * 512)
- Axial TSE T2 Fat Suppression (FS) (ST : 5 mm, TE:115 msec, TR: 4180 msec, FOV: 242 * 370 mm, Matrix: 512 * 336)
- Axial T2 BLADE (ST :3.5 mm, TE : 203 msec, TR :6150 msec, FOV: 250 * 250 mm, Matrix: 320 * 320)
- 3D Axial Constructive Interference in Steady State (CISS) (ST:2.2 mm, TE: 4.2 msec, TR: 8.5 msec, FOV: 199 * 199 mm, Matrix: 384 * 384)
- T2 DIXON FS and Water Suppression (WS) (ST: 3.5 mm , TE : 64 msec, TR: 3710 msec, FOV: 199 * 199 mm, Matrix: 384 * 384)
- T1 DIXON FS and WS (ST: 3.5 mm, TE :15 msec, TR : 561 msec, FOV: 220 * 220 mm, Matrix: 384 * 384)

RESULTS

Ultrasound and MRI images revealed features of the cords and surrounding tissues and are summarized in *Tables 1 and 2*.

Ultrasound

During imaging, US displayed deformation of the dermis associated with tensioning cords during shoulder abduction (*Fig. 1a,b*) or elbow flexion and extension (*Fig. 1c,d*). US also distinguished an anechogenic appearance of cords that may have corresponded to the lumen of a vessel with a hyperechogenic edge representing probably vessel wall (*Fig. 1a*).

TABLE 2
Summary of Features Identified with MRI Imaging of Cords and Surrounding Tissues in 15 Patients

	*P1	P2	P3	P4	P5	P6	P7	P8	P9	P10	P11	P12	P13	P14	P15
No visualization			x	x	x		x	x					x		x
Detection		x				x			x	x	x	x		x	
Cord from the surgical site		x									x	x			
Correlation catheter tracking and cord		x				x			x	x	x	x		x	
Presence of a lymphocele		x							x						
Fluid nature		x													
Edema		x								x					
Thrombus										x					
Correlation MRI / Ultrasound		x				x			x	x	x	x		x	

*P = patient

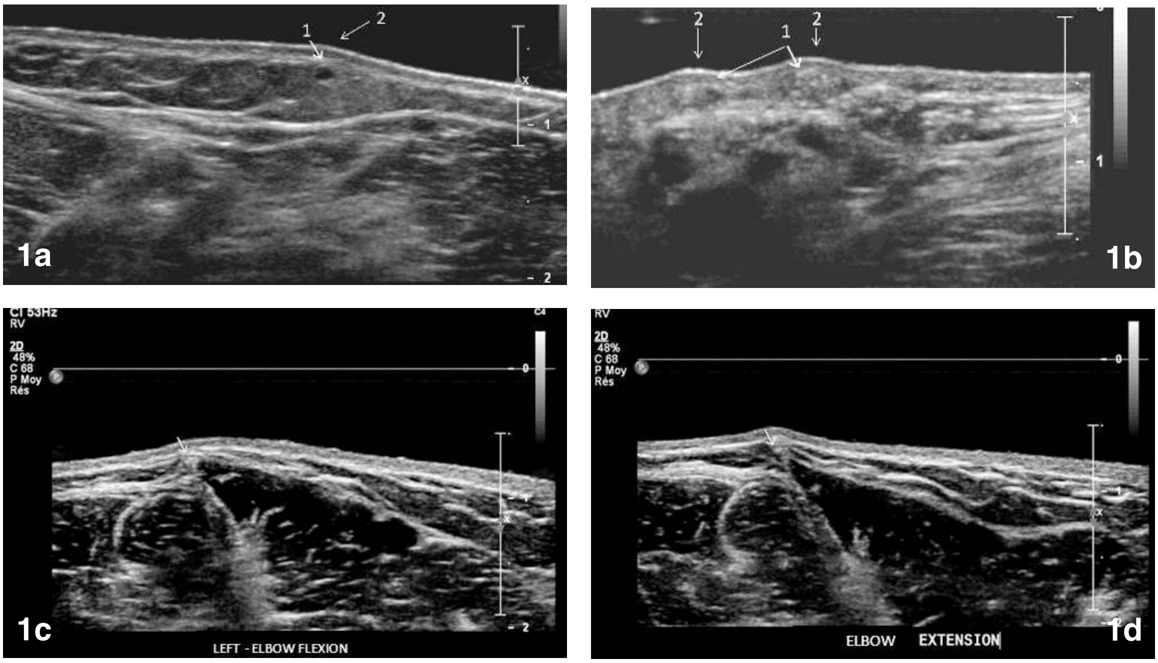

Fig. 1. US imaging of AWS displaying echogenicity of the cord and deformation of the dermis. The cord appears on US imaging like a string with an anechogenic lumen and a hyperechogenic edge representing the vessel wall (Fig 1a, arrow 1, shoulder in abduction). We detected a deformation on the surface due to the presence of an arch (Fig 1a, arrow 2, Fig 1b, arrows 2). A hyperechogenic aspect of the cord was in some cases detected (Fig 1b, arrow 1, shoulder in abduction) probably due to fibrosis. Hyperechogenic images of cords are illustrated (Fig. 1c and 1d) and detected with elbow in flexion (1c, arrow) and in extension, where we see also an arch on the surface (Fig. 1d, arrow).

We also observed hyperechogenic structure (*Fig. 1b*) probably corresponding to a cord fibrosis. These two aspects were found in 7 out of 15 patients. US also confirmed the precise location of the cord even if it was located deeper in the hypodermis fascia junction, as illustrated with abduction of the shoulder in *Fig. 2*. In longitudinal section,

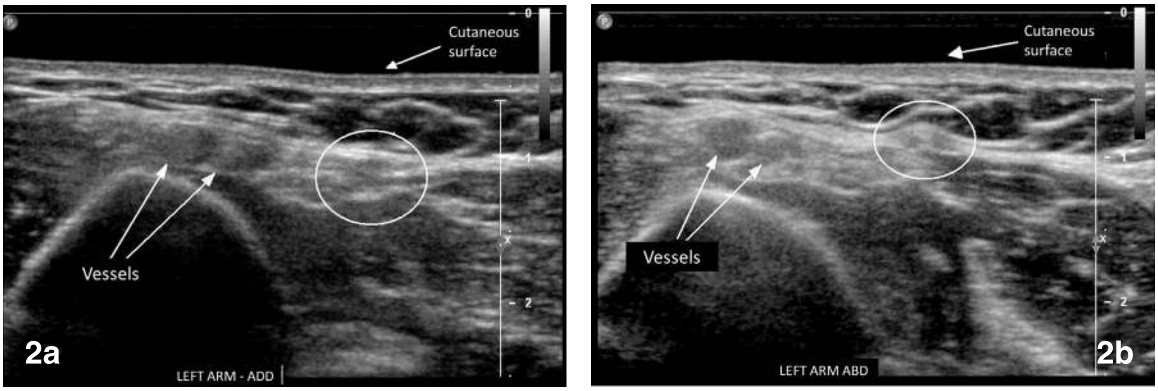

Fig. 2. US imaging of the cord in deeper localization. The cord is located at the hypodermis fascia junction detected with difficulty with shoulder in adduction (Fig 2a - center of the circle). Placing the shoulder in abduction helps enhance the arch and the cord (Fig 2b - center of the circle).

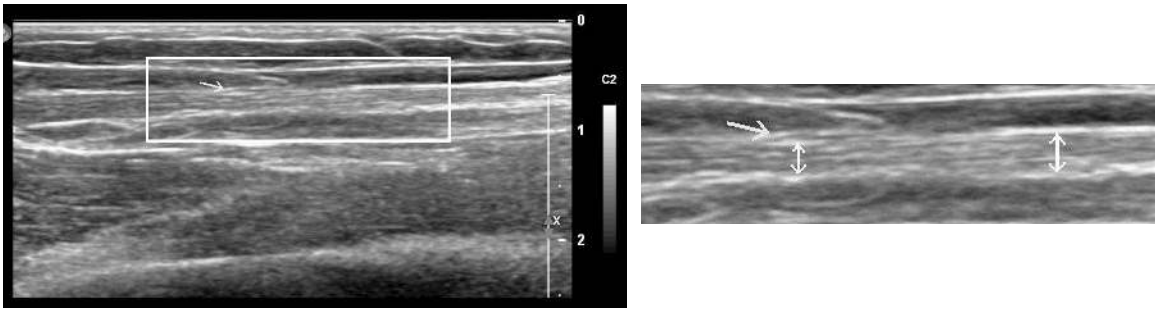

Fig. 3. US imaging of the AWS in a longitudinal section at the root of the arm. The cord corresponds to a hyperechogenic linear structure extending along the axis of the arm (arrow in the rectangle). In the zoomed rectangle (right side of the figure 3), the verticals arrow between both linear hyperechogenic structures define the width of the cord.

Fig. 4. US Color Doppler imaging of the edematous infiltration and endoluminal thrombus. Echographic aspect of hyperechogenic infiltration (rectangle) and of endoluminal thrombus (arrow 1). Blood vessels are detected by means of color Doppler (arrow 2).

the cord can also correspond to a hypodermic hyperechogenic linear structure extending along the axis of the arm (*Fig. 3*).

In four subjects, we found a hyperechogenic edematous infiltration *(Fig. 4, rectangle 3*). This same image also shows another aspect: an anechogenic area with a hypoechogenic content that suggests the presence of an endoluminal thrombus *(Fig. 4, arrow 1*). We found this image in 8 out of 15 patients. The presence of blood vessels (*Fig. 4, arrow 2*) observed in a color Doppler mode helped to clarify the position of the cord for the MRI image comparison. Moreover, blood flow was easily detected by its speed. By contrast, the extremely slow lymphatic flow was impossible to detect. Viewing a flow in a cord image detected on Doppler would invalidate the lymphatic origin of the cord.

Fig. 5. MRI image obtained using the Axial 3D T2 CISS sequence at the root of the arm demonstrates ferromagnetic artifacts joined by the cord in the axilla.

Fig. 6. (a) MRI image obtained using the Axial T2 3D CISS sequence displaying the cord with marking by the catheter. (b) MRI image obtained using T2 BLADE sequence displaying the cord (1), catheter (2), ferromagnetic artifacts (3), and vascular bundle (4).

Magnetic Resonance Imaging

MRI images displayed the cord to the adenectomy area. The axilla incised during the nodal sampling was also detected through ferromagnetic artifacts detected using 3D Ciss T2 mode during an axial section performed at the root of the arm (*Fig. 5*). Placement of the surface catheter to mark the cord identified by palpation allowed identification of the cord relative to other tissues (*Fig. 6, arrows*) although the mark may move slightly when the arm is brought from shoulder abduction to adduction along the body. Some patients exhibited an axillary lymphocele. The T2 TSE ws DIXON (water suppression) technique was used to specify the fluid nature of the structure corresponding to the lymphocele, and the hyposignal after suppression confirmed its fluid composition (*Fig. 7, seroma arrow*). The T2 TSE fs DIXON (fat suppression) technique *(Fig. 8,*

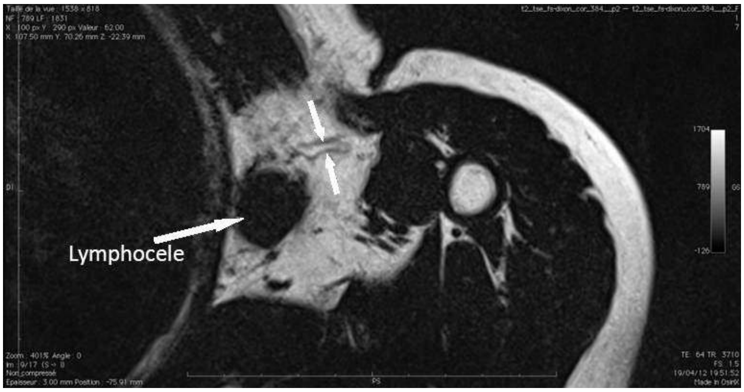

Fig. 7. MRI image obtained using a T2 TSE WS DIXON sequence (water suppression) displays a hyposignal lymphocele (long arrow) with a cord (highlighted by two short arrows) that extends into the lymphocele.

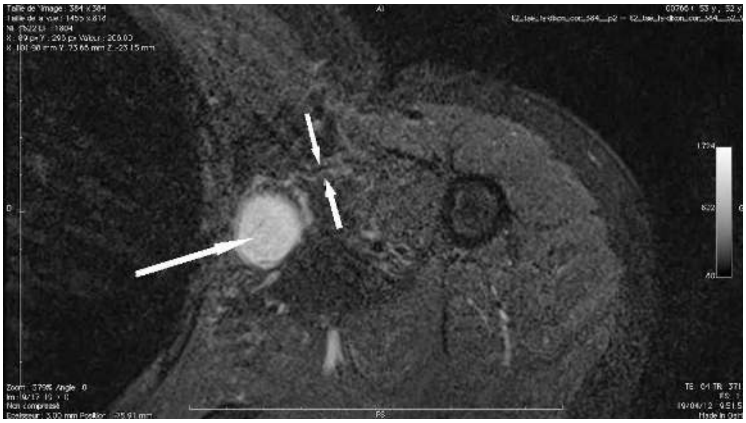

Fig. 8. MRI image obtained using a T2 TSE FS DIXON sequence (fat suppression) displays the seroma as hyperintense (long arrow) with the cord (short red arrows) extending into the lymphocele.

seroma arrow) eliminated the fat component of the and the remaining hypersignal confirms that it is not fat in the lymphocele. From these two observations, we can conclude that we are imaging a lymphocele and not an adenopathy. In the image sequences Dixon ws and fs (*Figs. 7 and 8, arrows*), we can follow the cords that extend into the lymphocele. With the Dixon sequences we obtain better images of the axilla than with conventional sequences in fat or water suppression. In fact, the exploration of the axillary crease under MRI proved to be extremely difficult from a technical point of view. The positioning of the small surface antenna on the arm was relatively difficult, especially when the arm was placed along the patient's body because the decentering of the antenna from the center of the magnet affected the efficiency of the classic and fat-suppressed sequences (FS: fat Sat) and did not always allow the exploration of the targeted region. Dixon sequences tolerate a greater decentering of the magnetic field. That is the reason why we used this sequence for imaging the axilla.

The identification of a thrombus in the cord is made possible through the combined use of different MRI sequences. The MRI cord slices performed every 3.5 mm indicate

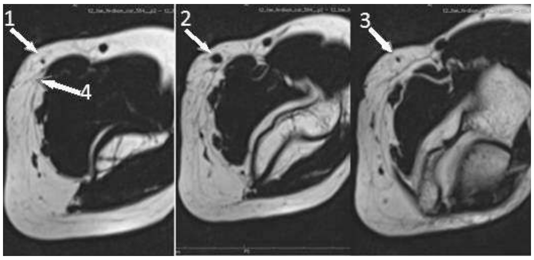

Fig. 9. MRI image obtained using a T2 TSE FS DIXON sequence (fat suppression) displaying a cord thrombus of changing diameter in 3 consecutive 3.5 cm slices (arrows 1, 2 and 3). In addition, depiction of the lymphedematous "honeycomb pattern" (arrow 4) can also be seen in the arm.

Fig. 10. Clinical picture of a patient in shoulder abduction displaying visualization of three individual axillary cords.

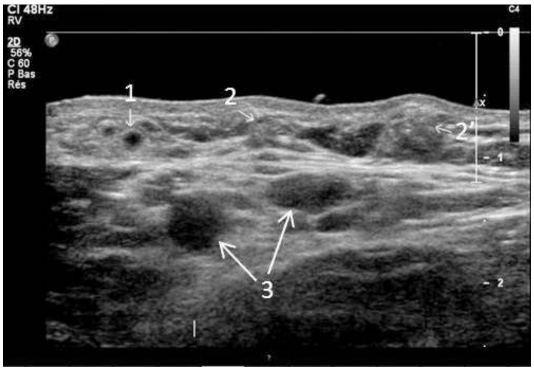

Fig. 11. US imaging of the same patient in Figure 10 demonstrates the three cords under the dermal arches (arrows 1, 2 and 2') near a vascular bundle (arrow 3).

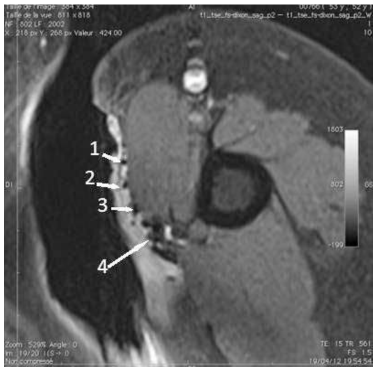

Fig. 12. MRI image obtained using a T1 TSE FS DIXON sequence in the same patient from Figures 10 and 11 demonstrate visualization of three cords (arrows 1, 2 and 3) near the vascular bundle (arrow 4).

the length of the thrombus. In the illustrated case (*Fig. 9*), the length of the thrombus is estimated between 6 and 9 mm. The thrombus is present on the three slices. We observed a proximal shrinkage of the cord (*Fig. 9 - arrow 1*) then an enlargement (*Fig. 9 - arrow 2*) and in the end a distal narrowing (*Fig. 9 - arrow 3*). We verified good agreement between MRI and US. Indeed, the thrombus and the edematous infiltration are visible on both types of imaging. Edema on MRI is characterized by the typical image of the "honeycomb pattern," i.e., the network appearance of interlobular bays (*Fig. 9, arrow 4*).

The correlation between clinical, US and MRI strengthens the interpretation of individual results. Observation and palpation of several cords leads to the search for similar MRI and US images. In one patient, 3 separate clinical cords were observed in the clinic (*Fig. 10*). On US, with shoulder abduction, there are three arches under which we distinguish three cords (*Fig. 11, arrows 1, 2 and 3*). These three cords are near a vascular bundle *(Fig. 11, arrow 3*). On MRI, the three cords are observed in hyposignal using a T1-TSE FS Dixon sequence (*Fig. 12, arrows 1, 2, 3*) near the vascular bundle (*Fig. 12, arrow 4*).

DISCUSSION

Ultrasound and MRI Results

The imaging techniques used in our study allowed us to identify a structure corresponding to the AWS cord. US appears to be more accurate than MRI for detecting AWS cords, although imaging analysis largely depends on the skill and experience of the operator and proper positioning can be essential. Several factors can explain better identification of the cord using US:

1) Spatial resolution. In US, spatial resolution depends on the type of sensor used and ultrasound beam angle of incidence relative to the structure. The high frequency (17MHz) ultrasound probe used in our study allowed a good spatial resolution of thin cord images. The utility of such high frequency probes to analyze the architecture of the subcutaneous tissue was demonstrated by Fornage in 1993 (12) and Cammarata et al in 1998 (13). However, despite good spatial resolution, it is sometimes difficult to visualize a structure on ultrasound if the ultrasonic waves are not perpendicular to the structure we wish to highlight and if its surrounding environment has the same echogenicity. In MRI, spatial resolution depends on the size of the elementary volume of the matrix, the voxel. The more we diminish the voxel and the more the signal/noise ratio (SNR) is reduced, the more proportional it is to the voxel volume. Thus, the gain in spatial resolution can be ineffective if the image is too "noisy" (SNR too low) due to too small a voxel. The contrast which corresponds to the variation in the signal intensity between two adjacent structures is also a factor of quality of the image. Acquisition time is important as well because the parameters chosen for its calculation influence either the spatial resolution, or the contrast, or the SNR. Ideally then, it is a matter of finding the best compromise between spatial resolution, SNR, contrast and an acceptable duration of examination (14).

2) Identification of the cords. The visual and palpatory identification of the cord in order to guide the ultrasound examination is probably more effective than MRI tracking with a small catheter filled with gel bonded to the surface of the skin above the cord. Indeed, the catheter may have been moved during the installation of the patient in the MRI tube or have been shifted due to the movement of the skin caused by abduction of the arm. This could explain why in some cases the targeted structure is not perfectly located in the centerline of the tracking catheter. In both imaging techniques a body mass index lower than 25 facilitates the detection of the cord. In the study by Leidenius et al in 2003 (2), they noticed that patients with AWS had an average BMI of 23 kg/m^2 and mentioned that "subcutaneous fat thickness would prevent adhesion of the skin to the surrounding tissue during the early phase of scar formation." Brandao et al in 2006 (7), and our study in 2009 (5) did introduce patients with a BMI above normal in their study. However, the detection of the cord was easier with a thin person, both by viewing and by palpation.

3) Dynamic display. The ability to create dynamic sequences (such as setting the arm in abduction and repositioning it in adduction) during the ultrasound examination made it easier to identify the cord than with MRI examination.

4) Duration of the examination. Since duration of US is less than that of the MRI, it was easier for subjects to maintain the arm abduction throughout this relatively short examination period whereas during the MRI sequences three subjects were unable to maintain the abduction due to the pain generated by the tightening of the cords.

5) Technical difficulty. Exploration of the axilla by MRI was technically very difficult. The positioning of the small surface coil on the arm was complicated, especially when the arm was placed along the patient's body because the decentering in relation to the center of the magnet affected the

fat-suppressed sequences efficiency and did not always allow the exploration of the desired region. It is for this reason that we have used Dixon sequences a majority of times to obtain images of the axilla. Moreover, tracking the cord from the arm to its axillary root requires a large field of view. The use of a body coil is less sensitive than surface coils with an inevitable loss in spatial resolution and SNR cannot be compensated by an increase in examination time, especially when the abduction position is uncomfortable for the patient in suboptimal immobility. Some sequences have been modified in order to better identify the cords. The use of gradient echo sequences (3D CISS) is justified because of their improved sensitivity for the detection of ferromagnetic artifacts, allowing easier location of the surgical site.

On US, the cord was found in twelve of the fifteen subjects in four different presentations: a hypodermic structure formed of hyperechogenic walls defining a hypoechogeinc or even anechogenic lumen, a hypodermic hyperechogenic structure, a hypoechogenic structure in the dermo-hypodermic junction, a hypodermic hypo or even anechogenic structure with a hyperechogenic intraluminal thrombus.

The first two presentations of the cord are in agreement with the observations reported by Matter et al in 2002 (15) and Leduc et al in 2005 (16). In their study, Matter and al state that it is possible to detect the presence of lymphatic vessels, or to observe their possible expansion and to analyze their content through a 12MHz probe. For their part, Leduc et al also conclude that it is possible to observe normal or dilated lymphatic vessels with a 13.5 MHz probe. These authors identify small collecting lymphatics as hyperechogenic hypodermic linear structures and large collectors like structures with a double hyperechogenic linear wall surrounding a central anechogenic space. In the present study, it appears that the cord can be more difficult to detect in the root of the limb because it merges with the environment that is also hyperechogenic. In the presence of a hypoechogenic or even anechogenic lumen within hyperechogenic walls, tracking the cord from different hyperechogenic tissues is possible. Setting the arm in abduction also helps to expose the cord through its tightening causing a bulge of the aponeurosis and of the skin surface of the arm. The third and fourth presentations of the cord are also in accordance with the results of Matter et al (15). According to these authors, the hypoechogenic image could correspond to the presence of a thrombus in the lymphatic vessel. This hypoechogenic appearance could result from the fact that the lymph contains few cells such as platelets and red blood cells. The fourth image showing a hyperechogenic thrombus in a hypoechogenic lumen supports this hypothesis. At the dermo-hypodermic junction, a state of fibrosis (hyperechogenic) of the cord could prevent its detection in the soft tissue (hyperechogenic). This could explain why in some cases the cord could not be located by ultrasound examination although it was visible and/or palpable. Torres Lacomba et al (17) explain that after axillary dissection and the ensuing lymphorrhea a partial interruption of the lymphatic transport and occlusion of the vessel lumen occur. The stagnation of the lymph creates an inflammatory reaction in the lumen which begins where the thrombus was formed (i.e., in the axillary crease) and moves along the vessel. This would lead to a loss of the elastic qualities of the collectors, augment their visibility, and increase the feeling of pain caused during the stretch. The thrombus appearance seen on US and MRI supports the hypothesis that a lymphatic thrombosis is an etiologic factor of the syndrome. Other authors also suggest its lymphatic origin (1,3,4,8,18). In the seventies, Moskovitz et al (1) performed lymphangiograms in patients which suggested the existence of a link between the path of some lymphatic vessels and that of the cords. They moreover proceeded to a cord biopsy which, in four patients, revealed the presence of fibrin within lymphatic vessels and superficial veins. On the basis of these observations, they proposed that AWS was caused by lymphovenous damage, stasis and hypercoagulability within axillary vessels resulting in thrombosis of large veins or of superficial lymphatics of the arm and in the formation of palpable cords. Similarly, Reedijk et al in 2006 (3), after performing a biopsy of subcutaneous nodules, identified the cause of the AWS as an obstruction of a lymphatic vessel followed by its recanalization (thus explaining its clinical resolution with time). Histological findings evoked different diagnoses including organized hematoma, a pseudoaneurysm or thrombotic occlusion and recanalization of a blood or lymph vessel. However, the lack of blood and of hemosiderin argued against the presence of a hematoma or of a pseudoaneurysm while the lack of any elastic wall excluded it was a blood vessel. Brandao et al in 2004 (7) and Wald et al in 2006 (19) detected through lymphoscintigraphic analysis the existence of stenosis (not a thrombosis) of lymphatic vessels as well as recanalization of these vessels after lymphatic drainage treatment. Torres Lacomba et al in 2010 (5) suggested that the AWS was a sign of damage to the lymphatic system and that manual lymphatic drainage (MLD) could be used in order to re-channel the vessels if the etiology was really lymphatic. Finally, Leduc et al in 2009 (5) established a correlation between the description of the cord path in patients and the anatomical observation of the superficial radial lymphatic pedicle path of the forearm and the bicipital pedicle path of the arm (median brachial) brought together in the nodes of the anterior scapular nodes. These findings suggest that the cords correspond to lymphatic vessels the path of which has been interrupted during axillary dissection. A hypothetical link between the intercostobrachial nerve and AWS was also raised by Moskovitz et al in 2001 (1) but 43% of the patients who had undergone nerve preservation had developed an AWS, which suggested that the nerve ligation did not contribute to the development of AWS. Moreover, Senofsky et al in 1991 (20) and Teicher et al in 1982 (21) recommend nerve conservation to minimize postoperative morbidity. Abdullah et al in 1998 (22) support this choice after having shown that nerve preservation reduces by approximately 30% the incidence of sensory deficit in patients at 3 months postoperatively. Salmon et al in 1998 (9) concluded that nerve preservation is not functionally necessary, as shown by their 18-month assessment. Moreover, in 1998, Salmon et al (9) demonstrated that the intercostobrachial nerve preservation or section has, in the long-term, no effect on the quality of the arm and shoulder function. Since AWS does have an impact on the arm function, we can assume that the nerve hypothesis is unlikely. In addition, in no case does the ultrasound image of the cord correspond to the descriptions of the multifascicular appearance of the peripheral nerves, even when of small size in high resolution. This allows us once again to eliminate the nerve hypothesis (23). For their part, Salmon et al in 2004 (24) suggested two hypotheses that whether related or not could be at the origin of the cords. According to the first hypothesis, incision and/or inflammation as a result of the irradiation of the clavi-pectoral-axillary fascia could generate scar retraction of the brachial fascia. Alternatively, the section and / or stenosis of the lymphatics due to the irradiation could cause the formation of a cord. However, in our study, no link between the cord and any fascia was observed. The tubular appearance of the cords on ultrasound and the absence of any focal fascial thickening on the cords path on MRI argue against this etiology. In addition, in the five subjects examined, none of them had received radiation therapy before the development of axillary cords, and only two of them were following this treatment at the time the experiments took place. Other etiologies have been mentioned by different authors: venous damage induced by thrombophlebitis, lymphatic duct damage due to aseptic lymphangitis (10), scar adhesions, and inflammation and fibrosis due to axillary tissue damage (dissection of fat support and connective tissue) (11). But there is still a lack of evidence for any of these hypotheses. On MRI scan of three patients, the cord appears to be heading toward the site of surgical ferromagnetic artifacts and in two patients towards an axillary lymphocele. Therefore, the syndrome might result from the section and/or injury of the axillary lymph vessel in the surgical area. If the cord originates in a lymphatic structure, the question can be raised why it does not appear after adenectomy in other sites such as the inguinal region. According to our observations, to ideally visualize AWS, abduction and external rotation of the shoulder, extension of the elbow and supination of the forearm with the wrist in extension are prerequisites. Under these conditions, the cord likely corresponding to the median brachial and anterior radial pedicle is stretched over its full length. For other body adenectomy areas, it is difficult to stretch so intensively a severed lymphatic pedicle.

CONCLUSION

Our results show that detection of the cord in patients treated for breast cancer is difficult with both imaging methods. However, US seems to be more sensitive than MRI to detect the AWS cord and has the advantage of producing a dynamic assessment. Four different types of cord image can be seen by echography: a hypodermic linear structure formed of hyperechogenic walls defining a hypoechogenic or even anechogenic lumen; a hypodermic hyperechogenic linear structure; a hypoechogenic linear structure at the dermo-hypodermic junction; and finally a hypodermic hypo- or even anechogenic structure with a hyperechogenic intraluminal thrombus. The echographic appearance of the cords is similar to that of the lymphatic vessels and on MRI, the cords seem to be heading toward the surgical site or to a lymphocele located in the axillary crease. These results are in favor of a lymphatic origin of the syndrome. The agreement between the clinical findings, the echography and the MRI reinforces our lymphatic hypothesis.

ACKNOWLEDGMENTS

We thank the patients for their generous collaboration. We extend our warm thanks to the Department of Radiology of the Vesale Hospital for the provision of the equipment for the study.

REFERENCES

1. Moskovitz, AH, BO Anderson, RS Yeung, et al: Axillary web syndrome after axillary dissection. Am. J. Surg. 181 (2001), 434-439.
2. Leidenius, M, E Leppanen, L Krogerus, et al: Motion restriction and axillary web syndrome after sentinel node biopsy and axillary clearance in breast cancer. Am. J. Surg. 185 (2003), 127-130.
3. Reedijk, M, S Boerner, D Ghazarian, et al: A case of axillary web syndrome with subcutaneous nodules following axillary surgery. Breast 15 (2006), 411-413.
4. Torres Lacomba, M, MJ Yuste Sanchez, A Zapico Goni, et al: Effectiveness of early physiotherapy to prevent lymphoedema after surgery for breast cancer: Randomised, single blinded, clinical trial. BMJ 340 (2010), b5396.
5. Leduc, O, M Sichere, T Snoeck, et al: Axillary web syndrome: Nature and localization. Lymphology 42 (2009), 176-181.
6. Kepics, JM: Physical therapy treatment of axillary web syndrome. Rehab. Oncol. 22 (2004), 21-22.
7. Brandão, R, S Jordão, N Duarte, et al: Drenagem linfatica manual, com e sem anti-inflamatorios não esteroides, em associacão com o tratamento convencional de fisioterapia, na “thromose: linfatica superficial. Re(habilitar). 3 (2006), 87-108.
8. Ferrandez, JC, M Doyer, D Serin, et al: Thromboses lymphatiques superficielles. In: *Cancer du sein et médecine de rééducation*. Petiot S, Herisson C, Pelissier J (Ed.). Paris: Elsevier Masson; 2007, p158
9. Salmon, R, Y Ansquer, B Asselain: Preservation versus section of intercostal-brachial nerve (IBN) in axillary dissection for

breast cancer - a prospective randomized trial. Eur J Surg Oncol. 24 (1998), 158-161.
10. Lauridsen, MC, P Christiansen, IB Hessov: The effect of physiotherapy on shoulder function in patients surgically treated for breast cancer: A randomized study. Acta Oncol. 44 (2005), 449-457.
11. Fourie, WJ, KA Robb: Physiotherapy management of axillary web syndrome following breast cancer treatment: Discussing the use of soft tissue techniques. Physiother. 95 (2009), 314-320.
12. Fornage, BD. From 7,5MHZ to 20MHz and beyond: Sonography of the skin and subcutaneous tissues. J.E.M.U. 19 (1998), 184-188.
13. Cammarota, T, F Pinto, A Magliaro, et al: Current uses of diagnostic high-frequency US in dermatology. J. Radiol. 27 (1998), 215-223.
14. Kastler, B, D Vetter: *Comprendre l'IRM : Manuel d'auto-apprentissage*. Paris : Elsevier Masson, 4ième éd. ; 2006. p382.
15. Matter, D, E Grosshans, J Muller, et al: Apport de l'échographie à l'imagerie des vaisseaux lymphatiques par rapport aux autres méthodes. J. Radiol. 83 (2002), 599-609.
16. Leduc, O, E Fumière, L Brognard, et al: Imagery of the lymphatic system by means of echography and magnetic resonance. Lymphology 15 (2005), 1-6.
17. Torres Lacomba, M, O Mayoral del Moral: Les thromboses lymphatiques superficielles à l'origine du syndrome douloureux myofascial après curage axillaire pour cancer du sein. Kinésither. Scient. 494 (2008), 25-29.
18. Cocilovo, C, S Boolbol, E Valdes, et al: Less is more: Transmammary axillary lymph node evaluation: An initial clinical experience. Am. J. Surg. 192 (2006), 478-480.
19. Wald, M, H Krizova, J Adamek, et al: Lymphatic vessel "overload" on the arm after axial dissection. EJLRP 12 (2004), (41 Sp. Co. I) 43.
20. Senofsky, G, FL Moffat, K Davis, et al: Total axillary lymphadenectomy in the management of breast cancer. Arch. Surg. 126 (1991), 1336-1341.
21. Teicher, I, B Poulard, L Wise: Preservation of the intercostobrachial nerve during axillary dissection for carcinoma of the breast. SGO. 155 (1982), 891-892.
22. Abdullah, TI, J Iddon, L Barr, et al: Prospective randomized controlled trial of preservation of the intercostobrachial nerve during axillary node clearance for breast cancer. Br. J. Surg. 85 (1998), 1443-1445.
23. Bianchi, S: Échographie Des Nerfs Périphériques. Revue du Rhumatisme. 75 (2008), 911-917.
24. Salmon, RJ, JP Hamelin: Maladie de Mondor: Vers une nouvelle explication physiopathologique et son traitement. Oncol. 6 (2004), 477-480.

Professor Olivier Leduc, PhD
Lympho-Phlebology Department of Occupational and Environmental Physiology
Haute Ecole P. H. Spaak, Brussels
University of Brussels, Institut Jules Bordet, Lymphology Unit
26 Avenue Des Di Arpents
Brussels, BELGIUM 1200
Telephone #: 0032 2 7790054
FAX #: 32 2 7792088
e-mail: olivierleduc@skynet.be